



ELSEVIER

Journal of Non-Crystalline Solids 263&264 (2000) 342–357

JOURNAL OF  
NON-CRYSTALLINE SOLIDS

www.elsevier.com/locate/jnoncrystol

## Continuous melting of phosphate laser glasses

J.H. Campbell<sup>a,\*</sup>, T.I. Suratwala<sup>a</sup>, C.B. Thorsness<sup>a</sup>, J.S. Hayden<sup>b</sup>, A.J. Thorne<sup>b</sup>,  
J.M. Cimino<sup>b</sup>, A.J. Marker III<sup>b</sup>, K. Takeuchi<sup>c</sup>, M. Smolley<sup>c</sup>, G.F. Ficini-Dorn<sup>d</sup>

<sup>a</sup> Lawrence Livermore National Laboratory, P.O. Box 808, Livermore, CA 94550, USA

<sup>b</sup> Schott Glass Technologies, 400 York Ave., Duryea, PA 18642, USA

<sup>c</sup> Hoya Corporation, USA, 3400 Edison Way, Fremont, CA 94538-6190, USA

<sup>d</sup> Centre d'Etudes de Limeil-Valenton, EME/ECO, 94795 Villeneuve St. Georges cedex, France

### Abstract

Continuous melting of phosphate laser glass is being used for the first time to prepare meter-scale amplifier optics for megajoule lasers; a description of the melting process is given. Two key factors in the successful melting of laser glasses are the elimination of damage-causing Pt-inclusions and dehydroxylation of the glass to concentrations less than ~100 ppmw OH. Oxidizing conditions using 100% O<sub>2</sub> or O<sub>2</sub> + Cl<sub>2</sub> mixtures (at one atmosphere) can be used to dissolve Pt inclusions and the effects of different gases on the dissolution of Pt-inclusions show the trend O<sub>2</sub> + Cl<sub>2</sub> > O<sub>2</sub> ≫ N<sub>2</sub>. The removal of hydroxyl groups is achieved by reactive (O<sub>2</sub> + Cl<sub>2</sub>) or non-reactive (O<sub>2</sub>) gas bubbling; model calculations are used to simulate this process. © 2000 Published by Elsevier Science B.V. All rights reserved.

### 1. Introduction

Continuous laser glass melting is being used for the first time to supply glass for large laser systems designed for fusion energy research [1,2]. One of these laser systems is under construction in the US [1] and a second is planned for construction in France [2]. The US facility is called the National Ignition Facility (NIF); the name is derived from its purpose: to achieve controlled thermonuclear (fusion) ignition. The French laser system is called the Laser MegaJoule (LMJ).

The NIF laser will be capable of delivering nearly 1.8 MJ of energy in about a 3.5 ns pulse, giving a peak power of approximately

$5.0 \times 10^{14}$  W. To achieve this output, NIF uses 192 individual laser beamlines each of which contains 16 Nd-doped laser glass plates (Fig. 1). More than 3000 glass plates will be installed on the NIF. Similarly, the planned French laser will require nearly 4500 glass plates. Thus, almost 8000 laser glass plates will be needed for the two laser systems: this represents a volume in excess of 125 m<sup>3</sup> (330 metric tons) of *finished* optical quality glass. Note that the quantity of raw glass that must be melted is larger than 330 metric tons to account for various process losses.

In contrast to the 1.8 MJ NIF and LMJ laser systems, the largest Nd-glass lasers currently in operation are the 70 kJ Nova (LLNL) [3] and the 40 kJ Omega [4] (University of Rochester) laser systems. These two systems use only about 2.2 and 1.1 m<sup>3</sup> of laser glass, respectively. In addition, the largest size Nd-glass amplifier disks installed on these two lasers are the 7 ℓ (46 cm aperture) elliptical

\* Corresponding author. Tel.: +1-925 422 6497; fax: +1-925 423 0792.

E-mail address: cambell12@llnl.gov (J.H. Campbell).



Fig. 1. One of the 3072 laser glass optics that will be used on the 1.8 MJ NIF laser. Each optic is about  $81 \times 46 \times 4$  cm<sup>3</sup> and is comprised of a rectangular plate of either LHG-8 or LG-770 Nd-doped phosphate laser glass. The edges of the plate are edge-clad with 1.2 cm thick strips of an index-matching Cu-doped phosphate glass. Each optic can store about 3.5 kJ of energy.

disks on Nova and the 2  $\ell$  (21 cm aperture) disks on Omega. Therefore, the combined NIF and LMJ lasers require approximately 75 times the laser glass production capacity used for Nova and Omega with glass-part sizes more than 2 times larger.

Both the NIF and LMJ laser systems employ a compact laser amplifier design called the ‘multi-segment amplifier’ (MSA) [5–8]. These amplifiers consist of stacked  $4 \times 1$  arrays of laser glass plates inside a flashlamp-pumped cavity. By using square apertures (i.e., square beams), it is possible to tightly pack the individual laser glass amplifiers into a compact matrix and greatly reduce the size and cost of the system [1,8]. This design requires that the laser glass be manufactured in rectangular plates (Fig. 1) [9]. Note that although the laser aperture is square, the laser glass plates are rectangular because they are mounted at Brewster’s angle to the propagation direction of the beam. Mounting the glass at Brewster’s angle minimizes the Fresnel reflection losses at the slab surfaces [10]. In addition, mounting at an angle increases the coupling efficiency of the flashlamp-pump light with the slabs [5,10].

In this paper, we first summarize the composition and properties of the two laser glasses to be

used in the megajoule lasers and then describe the advanced continuous optical glass melting systems that have been developed to produce these laser glasses. The remaining sections of the paper describe technical advances in understanding two of the key processing steps that affect the laser glass performance: (1) elimination of metallic Pt-inclusions that might induce laser damage and (2) reduction in concentration of hydroxyl groups that shortens the Nd<sup>3+</sup> fluorescence lifetime.

Continuous laser glass melting systems, based on the technology described here, have been constructed and are currently producing glass at both Schott Glass Technologies and Hoya Corporation, USA.

## 2. Laser glass composition and properties

The laser glasses used in the large laser amplifiers are Nd-doped metaphosphate glasses [11]. The two specific glasses that meet the gain, energy storage, extraction efficiency and damage resistance requirements of NIF and LMJ [11–13] are LHG-8 (Hoya Corporation) [11,14–17] and LG-770 (Schott Glass Technologies) [11,12,14,17,18]. The composition and key properties of LHG-8 and LG-770 are summarized in Table 1 and the Nd<sup>3+</sup> absorption and emission spectra of the two glasses are given in Fig. 2. Campbell and Suratwala [11] have reviewed recent advances in Nd phosphate laser glasses used for high-energy and high-peak-power applications; consequently, we will not discuss laser glass properties further here except as they directly relate to continuous melting.

The glass composition data (Table 1) are given on an oxide equivalent basis. Both glasses have near-metaphosphate compositions ( $O/P \sim 3$ ) and have very similar performance properties allowing them to be used interchangeably on the laser system. The major compositional difference in the two glasses is the group II modifier: LHG-8 contains BaO whereas LG-770 contains MgO. Both glasses use the same Nd-doping-level ( $4.2 \times 10^{20}$  ions/cm<sup>3</sup>).

The compositions given in Table 1 are listed as ranges and are intended to reflect the maximum

Table 1  
Composition and properties of Nd-doped phosphate laser glasses LHG-8 and LG-770 [14,16,17]

Composition <sup>a</sup> or property	LHG-8	LG-770
P <sub>2</sub> O <sub>5</sub>	55–60	58–62
Al <sub>2</sub> O <sub>3</sub>	8–12	6–10
K <sub>2</sub> O	13–17	20–25
BaO	10–15	–
MgO	–	5–10
Nd <sub>2</sub> O <sub>3</sub> <sup>b</sup>	0–2	0–2
Other	<2	<2
<i>O/P</i> (± 0.1)	3	3
<i>Optical</i>		
Refractive index <sup>c</sup>		
<i>n<sub>d</sub></i> (587.3 nm)	1.5296	1.5067
<i>n<sub>l</sub></i> (1053 nm)	1.5201	1.4991
Non-linear refractive index		
<i>n<sub>2</sub></i> (10 <sup>-13</sup> esu)	1.12	1.01
<i>γ</i> (10 <sup>-20</sup> m <sup>2</sup> /W)	3.08	2.78
Abbe number (±0.05)	66.5	68.4
<i>Laser</i>		
Emission cross-section (10 <sup>-20</sup> cm <sup>2</sup> ) (±0.2)	3.6	3.9
Radiative lifetime (zero-Nd) (μs) (±3)	365	372
Judd–Ofelt radiative lifetime (μs) (±10%)	351	349
Emission band width (nm) (±0.1)	26.5	25.4
<i>Thermal</i>		
Thermal conductivity, 90°C (W/mK) (±0.03)	0.58	0.57
Thermal diffusivity (10 <sup>-7</sup> m <sup>2</sup> /s)	2.7	2.9
Specific heat, <i>C<sub>p</sub></i> (J/gK) (±0.02)	0.75	0.77
Coeff. thermal expansion, 20–300°C (10 <sup>-7</sup> /K) (±3)	127	134
Glass transition temperature <sup>c</sup> , <i>T<sub>g</sub></i> (°C) (±5)	485	460
<i>Mechanical</i>		
Density (g/cm <sup>3</sup> ) <sup>c</sup> (±0.01)	2.83	2.59
Poisson's ratio (±0.01)	0.26	0.25
Fracture toughness (MPa m <sup>1/2</sup> ) (±0.02)	0.51	0.43
Hardness (GPa) (±0.10)	3.43	3.58
Young's modulus (GPa) (±1.0)	50.1	47.3

<sup>a</sup> Range in composition values reflect variations due to Nd-doping concentration, melt volatility, and batching variations.

<sup>b</sup> Nd-doping levels typically <2 mol% Nd<sub>2</sub>O<sub>3</sub> (<5 × 10<sup>20</sup> Nd ions/cm<sup>3</sup>); the NIF and LMJ use a doping of 4.2 (± 0.1) × 10<sup>20</sup> ions/cm<sup>3</sup>.

<sup>c</sup> Values may vary slightly with Nd-doping level.

variability in composition that can occur due to volatile losses, different Nd-doping levels and batching variations. In addition, this protects certain proprietary aspects of the exact composition. However, once the continuous melting conditions are established the composition variation is insignificant as indicated by the very small index fluctuations in the product glass over any 24 h

period (≤ ± 0.0001) and confirmed by chemical analysis of the product glass.

Note that small ranges in phosphate laser glass composition, such as those shown in Table 1, have little effect on the key laser properties. LHG-8 and LG-770 have nearly identical properties (see Table 1 and Fig. 2) yet their range of compositions and modifiers differs. Campbell and Suratwala [11]

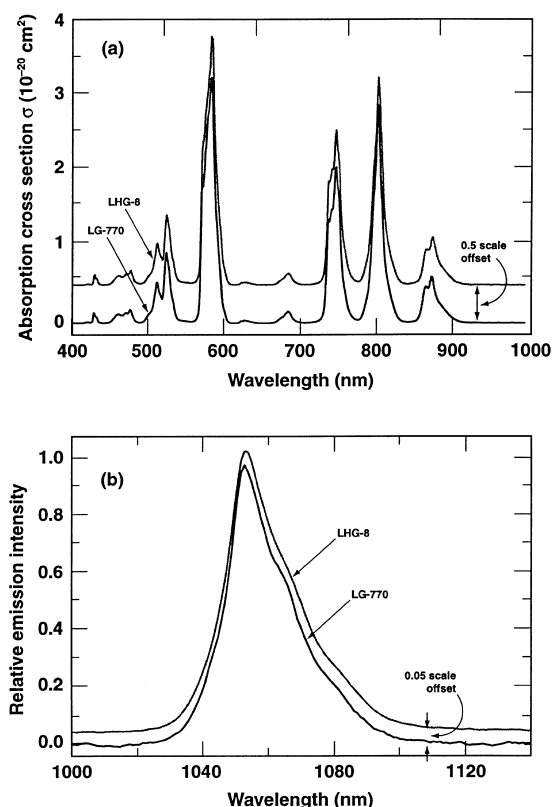


Fig. 2. Absorption (a) and emission (b) spectra for  $\text{Nd}^{3+}$  in the two phosphate laser glasses LHG-8 and LG-770.

have reported a similar insensitivity of most properties to minor changes in composition for laser glass having the approximate composition  $60\text{P}_2\text{O}_5-10\text{Al}_2\text{O}_3-30(\text{M}_2\text{O}/\text{MO})$ . As regards this particular manuscript, the range of compositions shown does not affect the results and conclusions given here for continuous glass melting.

### 3. Discontinuous melting

To put in perspective the scale of the continuous laser glass melting process, it is instructive to briefly describe the older discontinuous process [19,20]. In the past, the glasses made for the large ICF laser systems (e.g., Nova [LLNL], Phebus [CEA], Beamlet [LLNL], Gekko [Osaka], and Omega [University of Rochester]) [12] were manufactured using a one-at-a-time, discontinuous

melting system. The first step of the discontinuous process is a pre-melting step designed to melt and mix (on a large-scale length) the raw materials (Fig. 3). A gas is often bubbled through the pre-melt to remove unwanted volatile products, particularly water and, if necessary adjust the melt redox state. The pre-melt is carried out in a relatively inert refractory crucible such as  $\text{SiO}_2$ . The walls of the refractory vessel dissolve over time eventually requiring the vessel to be replaced. The glass from the pre-melter generally contains bubbles, striae, and, occasionally, some small particles of unmelted starting material.

The product glass from the pre-melt stage is next processed in a physically separate unit called the 'remelter'. The remelter is a platinum-lined refractory vessel that also has provisions for stirring and gas bubbling. The main purpose of the remelter is to dissolve any platinum-inclusions, remove bubbles and finally, improve the homogeneity of the glass to provide the striae-free, optical quality glass necessary for laser applications. The remelting process occurs in several stages [19]. During the first stage, the redox state of the glass is adjusted to increase platinum particle dissolution [21]. This step is followed by a refining process conducted at temperatures greater than  $1050^\circ\text{C}$  at which the viscosity of the glass is  $<10$  poise, allowing bubbles to rise to the surface. The third

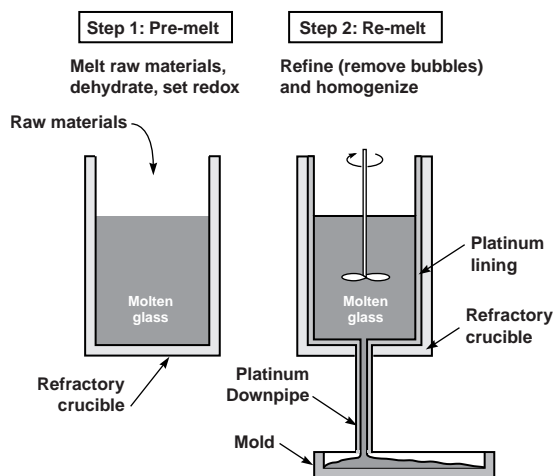


Fig. 3. Schematic representation of the discontinuous, 2-step melting process formerly used to produce laser glass.

stage is a stirring process that is generally conducted at temperatures lower than either the melting or the refining stages. The continuous stirring thoroughly distributes all components within the glass melt, eliminating striae and increasing the uniformity of the refractive index over the entire casting. Finally, the melt is cooled to a temperature such that the viscosity of the glass is proper for casting into a mold of the appropriate size and shape. After casting, the glass undergoes an initial, relatively rapid annealing step, is inspected for inclusions and striae, and then is again annealed at a slower rate (several weeks) to reduce any residual thermal stresses.

Discontinuous processing methods have been used with good results for producing small quantities of laser glass. However, the discontinuous process has a small through-put and a single melting system can, at best, only produce a few glass plates per week (<5) [19,20]. In addition, the quality of the product glass can vary from one melt to the next simply because of small, but random, run-to-run variations in processing conditions. Continuous glass melting, on the other hand, has the advantage that not only can a much greater production rate be achieved but, in addition, once steady-state is achieved, there is little if any measurable variation in glass properties from one glass plate to the next.

#### 4. Continuous glass melting

Continuous optical glass melting systems are generally divided into several interconnected zones [20,22]. Each zone consists of one or more vessels designed to carry out a particular part of the process. In the specific case of the laser glass continuous melters, there are six main interconnected processing zones (Fig. 4): (1) raw material mixing and feeding, (2) melting, (3) conditioning, (4) refining, (5) homogenization and (6) continuous strip forming. Each of these is described briefly below.

##### 4.1. Laser glass raw material, mixing and feeding

The glass transmission losses at the laser wavelength (1054 nm) must be very low ( $\lesssim 0.0015 \text{ cm}^{-1}$ ). Therefore the purity requirements for the raw materials are very demanding. In particular, only trace amounts (few ppm) of most transition metal ions are permitted [23–26]. Although Cu has the highest measured absorption loss at 1054 nm, Fe is perhaps the most troublesome impurity to control because most processing equipment uses iron-based metals. Therefore, the purity requirements affect the choice of the raw material processing equipment and procedures. As an example, Table 2 gives the purity requirements for the Nd

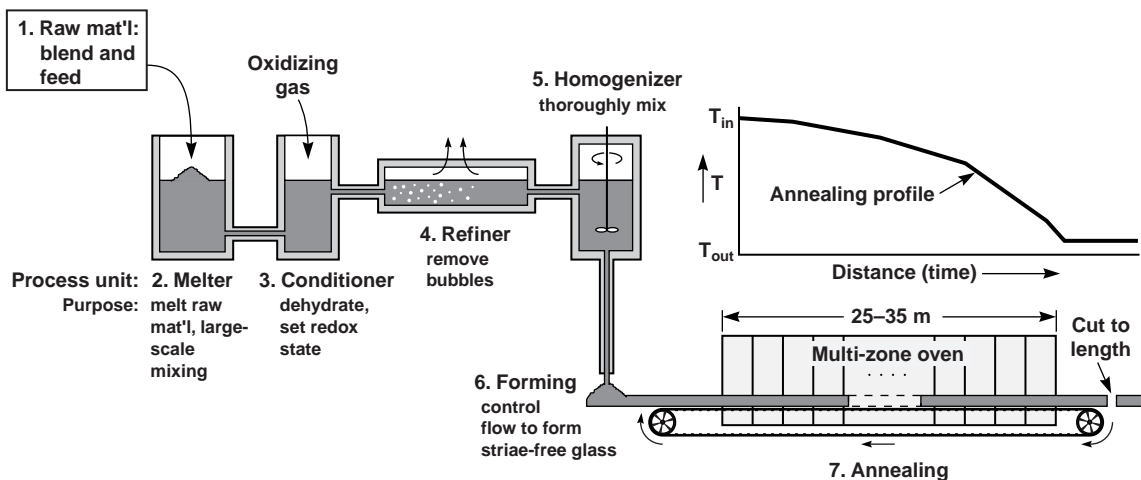


Fig. 4. Schematic representation of the continuous laser glass melting systems now being used to manufacture phosphate laser glass.

Table 2  
Metal ion purity for Nd salt (on oxide basis) used in laser glass melting

Element (as oxide)	Purity level (ppmw)	
	Specified (maximum)	Measured (typical)
Transition metals		
CuO	1	0.25
Fe <sub>2</sub> O <sub>3</sub>	2	1.3
CoO	1	0.05
NiO	1	0.44
V <sub>2</sub> O <sub>5</sub>	1	0.03
Cr <sub>2</sub> O <sub>3</sub>	1	0.42
Rare earths		
Pr <sub>6</sub> O <sub>11</sub>	100	18
La <sub>2</sub> O <sub>3</sub>	100	27
Sm <sub>2</sub> O <sub>3</sub>	30	0.9
CeO <sub>2</sub>	30	1.4
Dy <sub>2</sub> O <sub>3</sub>	10	<0.5
(Other rare earths)	10	<10

salt used in the melting process; the transition metal impurity levels are typical of the requirements for most of the raw materials. Unique to the Nd, however, is the low concentration of other rare earths (<100 ppmw) that is required. Rare earth ions are usually separated by a solvent extraction process [27]. This process can make the manufacture of a high-purity Nd salt quite difficult because the similar reaction chemistry among rare earths often makes the extraction process inefficient particularly for certain pairs of rare earth ions.

Compounding the difficulty of raw material purity is the need to achieve these levels for many tons of material. Recall from above that more than 300 tons of finished glass must be manufactured. Of course, much more than this must be melted to cover the yield and fabrication losses inherent in the process. The Nd raw material requirements alone consume most of the world-wide manufacturing capacity for high-purity Nd salt.

In addition to transition and rare earth elements, the raw materials should contain little physically or chemically absorbed water (<0.1 wt%) as this introduces hydroxyl groups in the glass that can increase the Nd non-radiative decay rate [11]. This requirement can be quite trouble-

some because of the inherent hygroscopic nature of some of the laser glass raw materials and the fact they are supplied as finely ground powders. The raw materials should be mixed in a dry atmosphere and then delivered continuously to the melter with precautions to avoid water uptake.

#### 4.2. Melting

The batch powder that enters the melter dissolves in the molten glass and undergoes large-scale mixing driven by convection currents within the melter. Off-gas handling equipment collects any gas emissions from the melter (or other vessels) and treats the effluent to meet environmental regulations.

Compared to silicate glasses, phosphate laser glasses generally melt in the range of 1000–1200°C. Heat is supplied to the melter by electrical means because gas-fired heat sources increase the concentration of hydroxyl groups in the glass.

The lifetime of the whole melting system is governed by the dissolution rate of the refractory walls of the melter unit. Phosphate glasses tend to be relatively corrosive to most refractories; therefore the choice of a proper refractory becomes a critical decision in the design of the melter system. This choice is made by comparing results from

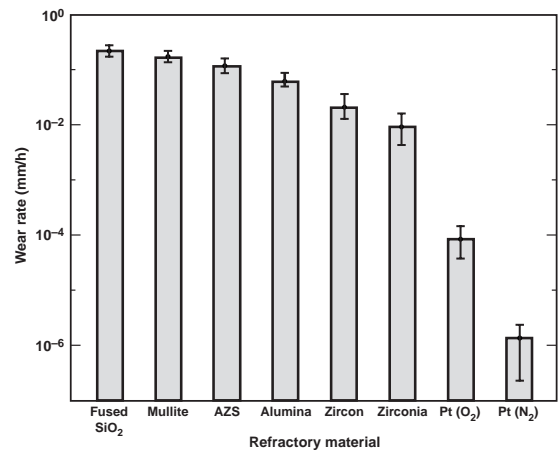


Fig. 5. Comparison of dissolution rates of various refractories with those for pure platinum (99.95%) in a metaphosphate laser glass melt (LG-750, see Table 3). Unless noted, all data are for melts in ambient air at 1300°C.

lab-scale measurements of the dissolution rate of candidate refractories exposed to the molten glass composition over the range of temperatures of interest. Fig. 5 compares the dissolution rate of a range of typical refractories when exposed to a metaphosphate laser glass at 1300°C. Also shown, for comparison, is the corrosion rate of Pt metal under both oxidizing and reducing conditions; this will be discussed further in the next section. The dissolution rate of the refractory is usually not uniform over the whole area exposed to the melt but tends to be greatest at the three-phase region where the melt surface contacts the refractory [28]. The melter refractory material must be high purity so as not to significantly add impurities into the melt. This includes not only dissolved impurities such as transition metals or –OH groups [11,24,26], but also particulate material or, as commonly labeled, ‘stones’ [21]. Table 3 summarizes the observed dissolution properties for the same set of refractories whose wear rate is shown in Fig. 5.

One advantage in melting phosphate glasses is that the dissolved refractory wall material can generally be easily identified in the glass matrix. Therefore, by periodically analyzing the product glass for dissolved refractory material, one can continuously monitor the melter wear rate and, using a simple mass balance, estimate the life remaining in the melter.

#### 4.3. Glass conditioning

All glass-processing sections beyond the melter (from the conditioner to the forming down-pipe,

see Fig. 4) use platinum-lined vessels. In addition, all interconnecting pipes, stirrers, etc., are also Pt. The Pt purity is >99.95% and is refined and processed into the needed shapes at a precious metal fabricator. Platinum is used in the melter systems because of its low wear rate (Fig. 5) and because the small quantity of ionic platinum that is introduced into the melt ( $\lesssim 100$ –200 ppm) has a negligible effect on the laser glass properties.

Apart from cost, the one major technical disadvantage in using platinum is the possible introduction of Pt-metal inclusions into the glass. For many years Pt-inclusions limited the output fluence of glass lasers because the interaction of the laser light with the inclusions generates fracture sites within the glass [21,29–31]. Processing conditions have since been developed that largely eliminated Pt-inclusions in phosphate glasses by controlling the redox state of the melt [32,33]. In fact, one of the major purposes of the conditioning unit is to adjust the redox state of the glass melt to increase Pt-inclusion dissolution. The redox state of the melt is controlled by addition of an oxidizing gas. Because of the size and continuous flow of the glass through this system, it is generally most efficient to bubble the oxidizing gas through the glass melt. Studies of platinum dissolution rates under oxidizing conditions show that O<sub>2</sub> [32,33], Cl<sub>2</sub> [33], Cl-containing gases (e.g., CCl<sub>4</sub> [33], POCl<sub>3</sub> [34]) or O<sub>2</sub> in combination with these gases can dissolve Pt-inclusions.

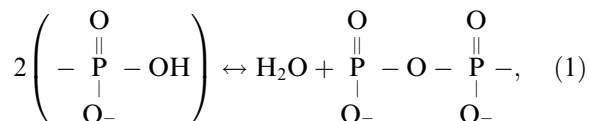
Bubbling gas through the glass melt has the added advantage of increasing the removal of –OH groups [35–38]. In the case of a non-reactive bubbling gas (e.g., O<sub>2</sub>) the removal is achieved by

Table 3  
Comparison of dissolution properties for various refractories exposed to a metaphosphate laser glass<sup>a</sup> at 1300°C [21]

Refractory material	Absorption at 1060 nm (10 <sup>-3</sup> cm <sup>-1</sup> ) (±1)	Wear rate (mm/h)	Refractory inclusions
Fused silica	3	0.28 ± 0.03	Few
Mullite	6	0.20 ± 0.03	Few
AZS (chrome)	15	0.11 ± 0.02	Several
AZS (fused)	7	0.07 ± 0.02	Several
Sintered alumina	5	0.06 ± 0.02	None
Zircon (medium density)	4	0.02 ± 0.01	Several
Zircon (dense)	7	0.02 ± 0.01	Few
Zirconia (fused)	27	0.01 ± 0.005	Many

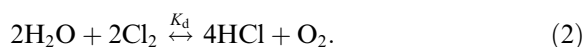
<sup>a</sup> LG-750 (mol%): (55–60)P<sub>2</sub>O<sub>5</sub>–(8–12)Al<sub>2</sub>O<sub>3</sub>–(13–17)K<sub>2</sub>O–(10–15)BaO–(0–2)Nd<sub>2</sub>O<sub>3</sub>.

equilibrium between the  $-\text{OH}$  in the glass and  $\text{H}_2\text{O}$  in the bubble as described by the reaction.



>where the OH equilibrium constant is proportional to the  $(P_{\text{H}_2\text{O}})^{1/2}$  [39,40]. The data in Fig. 6 are measured hydroxyl contents in LG-770 and LHG-8 glasses as a function of the water vapor partial pressure equilibrated with the glass. Equilibrium was achieved by bubbling an inert gas ( $\text{O}_2$ ) containing water vapor at a fixed vapor pressure through the glass melt at the temperatures shown in Fig. 6. The hydroxyl content is given in terms of the  $-\text{OH}$  absorption coefficient at  $3000 \text{ cm}^{-1}$  [40,41]. The slope of the data yields equilibrium constants of 0.41 and  $0.51 \text{ cm}^{-1}/\text{Pa}^{1/2}$  for LG-770 and LHG-8, respectively.

Reactive gases, such as the chlorine-containing gases mentioned above, are more effective than  $\text{O}_2$  because they react with the  $\text{H}_2\text{O}$  generated at the bubble interface via Eq. (1) and form HCl. For example, in the case of  $\text{Cl}_2$ , the governing reaction with  $\text{H}_2\text{O}$  is [42]



The equilibrium constant,  $K_d$ , for this reaction, known as the reverse Deacon reaction [42], favors the products (i.e.,  $K_d \gg 1$ ). Therefore the consumption of  $\text{H}_2\text{O}$  (i.e., OH) is much greater than can be achieved with a non-reactive gas. More specifically, when an inert gas such as  $\text{O}_2$  is used to 'dry' the glass then the factor limiting OH removal is the build-up of  $\text{H}_2\text{O}$  within the bubble. As soon as the  $\text{H}_2\text{O}$  level reaches equilibrium then a net mass transport of OH across the bubble interface stops. Furthermore, the smaller the OH content of the glass the quicker the bubble saturates and the less effective the drying process. On the other hand, a reactive gas such as  $\text{Cl}_2$  consumes  $\text{H}_2\text{O}$  at the bubble interface greatly increasing the drying capacity of the bubble. Of course, the equilibrium constant for Eq. (2) still governs the amount of  $\text{H}_2\text{O}$  consumed.

Further details of platinum particle dissolution and dehydroxylation are discussed in later sections

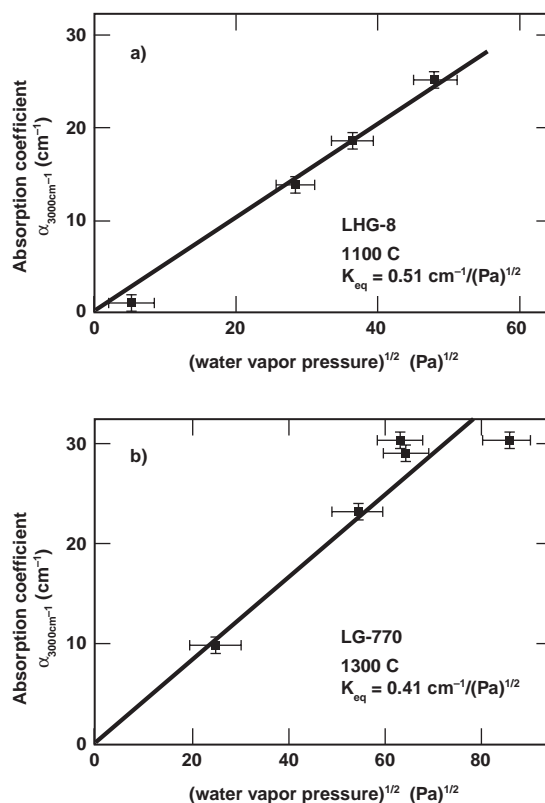


Fig. 6. Equilibrium hydroxyl content in (a) LHG-8 and (b) LG-770 metaphosphate laser glasses versus  $\sqrt{P_{\text{H}_2\text{O}}}$  at melt temperatures of  $1100^\circ\text{C}$  and  $1300^\circ\text{C}$ , respectively. The OH content is expressed in terms of the measured absorption coefficient at  $3000 \text{ cm}^{-1}$ .

because of their critical importance to the production of phosphate laser glasses.

#### 4.4. Refining, homogenization, and forming

The molten glass from the conditioning unit then flows to the refiner section where the temperature is elevated to reduce the glass viscosity and thereby increase the bubble rise velocity to promote bubble removal. This glass process, known as refining, is described in the literature (see, for example [22]).

The bubbles reach terminal velocity ( $v_t$ ) which is governed by a balance of forces due to buoyancy and viscous drag, and at steady state is described by the Stokes equation [43]

$$v_t = g(\rho_g - \rho_b)d_b^2/18\eta, \quad (3)$$

where  $\eta$  is the glass viscosity (poise),  $d_b$  the bubble diameter (cm),  $g$  the acceleration due to gravity ( $980 \text{ cm/s}^2$ ), and  $\rho_b$  and  $\rho_g$  is the density ( $\text{g/cm}^3$ ) of the gas in the bubble and the liquid, respectively. Phosphate glasses tend to have much lower viscosities at a given temperature than silicates (Fig. 7) with the result that bubble rise velocities are comparatively larger. Bubbles, in most cases, are not a problem in continuous melting of phosphate laser glasses.

The glass from the refiner next enters the homogenization section where Pt stirrers thoroughly mix the glass to achieve the part-per-million index homogeneity required for laser applications. Just as in the discontinuous process, the temperature of the homogenizing section is reduced to adjust the glass viscosity to give the desired flow properties needed to form a wide ( $\sim 50 \text{ cm}$ ), thick ( $\sim 5 \text{ cm}$ ), homogeneous strip of glass.

The combined width, thickness, and length of the glass strip produced during the forming operation is greater than any optical glass produced prior to continuous laser glass melting development. The technology used to ‘form’ (i.e., cast) the glass into a homogeneous continuous strip is proprietary and will not be discussed further here.

#### 4.5. Coarse annealing

Once successfully formed, the cast strip moves via a conveyer belt through a long (25–35 m) coarse annealing oven where the temperature is ramped down at a rate to avoid generating unacceptable thermal stresses in the glass. The coarse annealing step is typically much more of a challenge for phosphate laser glasses than other optical glasses because phosphate glasses have high coefficients of thermal expansions and low fracture toughnesses (Table 1). For example, compared to common commercial silicate optical glasses (e.g., BK-7 [44] or BSC-7 [45]), the thermal expansion coefficient of phosphate laser glasses is nearly twice as large and the fracture toughness only one-half as large. Therefore, the thermal shock resistance

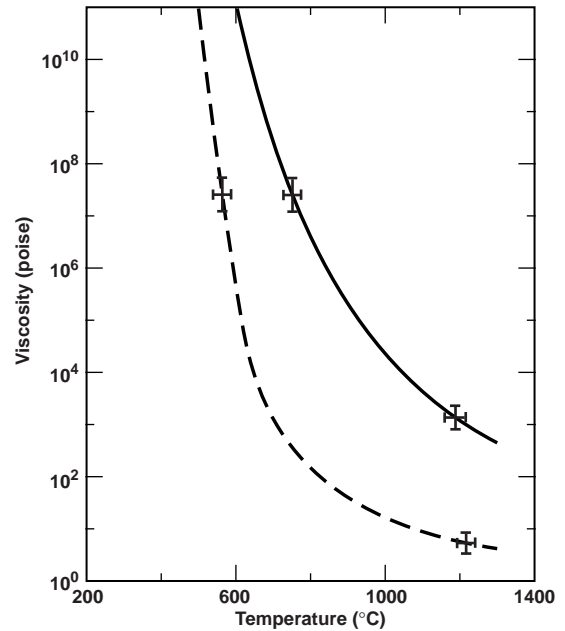


Fig. 7. Viscosity versus temperature for a typical silicate (solid line) and phosphate (dashed line) glass.

[11] of the phosphate laser glass is only about one-fourth that of BK-7, and the probability of fracture during coarse annealing and other post-processing steps becomes proportionally greater.

At the end of the coarse annealing oven, the continuous as-cast strip is cut into pieces that are then individually processed to give the desired laser glass plate.

#### 4.6. Glass processing after melting

There are four laser glass processing steps after melting: (1) final annealing, (2) optical metrology, (3) fabrication into prefinished blanks, and (4) cladding and final finishing. The first three steps are carried out at the glass manufacturers (Schott and Hoya) and the last step at an optical glass finishing company. The order in which various inspection, annealing, and fabrication steps are carried out may vary and depends on how each company has chosen to optimize their process.

The specified optical homogeneity and residual stress-induced birefringence of the laser glass re-

quire that it be annealed a second time at a much slower rate. During this second annealing step, called ‘fine annealing’, the glass plate is reheated to a temperature near the glass transition temperature ( $\sim 450\text{--}500^\circ\text{C}$ , see Table 1) and then slowly cooled over a period of several weeks ( $\geq 25$  days). Under these conditions the thermal gradients across the plate are small enough that residual stresses, as measured by the stress induced birefringence, are less than 5 nm/cm across the optic.

The laser glass must meet a given set of optical and laser performance criteria that are measured on each plate. Perhaps the four most important properties are: (i) index homogeneity, (ii) absorption loss at the laser wavelength, (iii) residual –OH content (specified by a maximum allowed absorbance at  $3000\text{ cm}^{-1}$ ) and (iv) platinum-inclusion content. The latter two are discussed in more detail in Sections 5 and 6, and the absorption loss is measured using standard spectroscopic transmission methods and thus is not discussed here. Instead we briefly discuss the index homogeneity measurements.

In the absence of residual stress, the homogeneity of the glass, as measured by variations in the refractive index ( $\Delta n$ ) is  $< \pm 2 \times 10^{-6}$ . The refractive index homogeneity of the glass is specified in terms of an allowable aberration in transmitted optical wavefront. This is measured directly on a 61 cm aperture, phase interferometer (Veeco Metrology). The interferometer measures the spatial variation in the phase of the transmitted wavefront that, in turn, is related to the refractive index homogeneity by

$$\Delta\phi(x, y) = \frac{2\pi\ell\Delta n(x, y)}{\lambda}, \quad (4)$$

where  $\Delta\phi(x, y)$  and  $\Delta n(x, y)$  are the spatial variation in phase (radians) and refractive index, respectively, when measured at wavelength,  $\lambda$  (m), using a glass of thickness,  $\ell$  (m). The magnitude of the allowed phase variation due to the glass inhomogeneity is usually expressed in terms of either the common set of optical aberrations (sphere, coma, astigmatism) or the set of orthogonal Zernike polynomials [46]. Note that in addition to specifications on the absolute magni-

tude of the phase error, there is also a limit on the magnitude of the phase gradient (i.e.,  $\delta\phi/\delta x$ ,  $\delta\phi/\delta y$ ). Measurement of glass index homogeneity is carried out in a fashion that eliminates phase error contributions from the front and back surfaces.

#### 4.7. Cladding and finishing

Each laser glass plate is eventually edge-clad with an index-matched glass containing a dopant ion ( $\text{Cu}^{2+}$ ) at a concentration sufficient to produce an absorption coefficient of  $0.28\text{ cm}^{-1}$  at 1054 nm [47]. The purpose of the cladding glass is to absorb emission from the spontaneous fluorescent decay of excited-state  $\text{Nd}^{3+}$ . These spontaneously emitted photons are amplified as they travel along the length of the glass plate either near the surface or by total internal reflectance. If these rays are not suppressed by a non-reflecting (i.e., index matched) edge-cladding then they can lead to parasitic laser oscillations which effectively de-excite the entire glass plate [47,48].

The cladding glass is produced using standard continuous strip melting operations in a separate melting system to avoid cross-contamination of the  $\text{Cu}^{2+}$  dopant into the laser glass. Nearly 20 metric tons (14 000 pieces) of cladding glass are needed to clad the roughly 3500 glass plates needed for the NIF laser system.

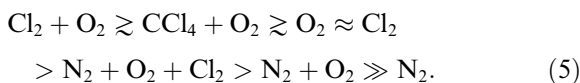
The cladding is bonded to the edges of the laser slab using a custom-formulated, index-matched, amine-cured epoxy [47]. The adhesive strength of the phosphate glass-to-epoxy bond is increased by use of a silane coupling agent [49]. Care is taken to avoid particulate (dust) contamination in the epoxy or on the bonded glass surfaces to eliminate sites for optical damage. Details of the cladding process are described elsewhere [47]; the process has been further developed so that glass plates can be automatically cleaned and clad using a combination of continuous and semi-continuous processing steps.

The cladding operations are the first step in final finishing. Once the cladding has been applied, the slab surfaces are ground and polished to achieve the overall transmitted wavefront quality needed for the laser.

## 5. Dissolution of damage-causing Pt-inclusions

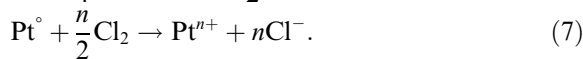
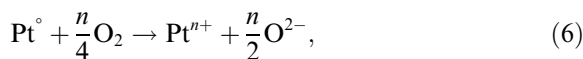
The operating fluence and irradiance of the megajoule scale lasers will be larger than any current laser system. Peak fluences in the laser glass will approach 18–20 J/cm<sup>2</sup> with a peak irradiance of about 5.0 GW/cm<sup>2</sup> [8]. To avoid optical damage the laser glass must be free of defects, specifically microscopic inclusions (either metallic or ceramic) left from the melting process. The most common inclusion source is metallic Pt-inclusions from the Pt-lined vessels used in the melting system [21]. Prior to about 1988, Pt-inclusion damage represented the major source of damage in laser glass used for peak-power application. However new processing methods have been developed that reduce the Pt-inclusion concentration by more than 1000 fold to <0.1 per liter [32,33].

The process for eliminating Pt-inclusions relies on the intrinsic property of many phosphate glasses to dissolve Pt metal under oxidizing conditions. Rindone and Rhoads [50] and Ryder and Rindone [51] were the first to report increased platinum dissolution in phosphate glasses with the addition of O<sub>2</sub> and Cl<sub>2</sub>. Izumitani et al. [34] have reported the use of gaseous POC<sub>3</sub> as an oxidizing additive, and Campbell and co-workers [21,32,33] studied the effects of O<sub>2</sub>, Cl<sub>2</sub>, CCl<sub>4</sub> and N<sub>2</sub>/O<sub>2</sub> mixtures. The rate of Pt dissolution follows the approximate trend [21,33]:



The measured rate of platinum dissolution at 1100°C as a function of both O<sub>2</sub> partial pressure and different gas additives, based on data from Campbell et al. [21], is shown in Fig. 8.

The proposed reactions [32,33] governing Pt dissolution in either O<sub>2</sub> or Cl<sub>2</sub> containing additives are



In the absence of O<sub>2</sub> (or Cl<sub>2</sub>) as gas additives, the oxidation is controlled by the equilibrium oxygen fugacity of the glass melt.

Ionic platinum gives the glass a slight yellow color due to its optical absorption below 450 nm. Correlation of ionic platinum content with the absorption at 400 nm has been reported [21]

$$[\text{Pt}^{n+}] = k \alpha_{400} - 1.6, \quad (8)$$

where [Pt<sup>n+</sup>] is the ionic platinum content in the glass (ppmw), α<sub>400</sub> the absorption coefficient (cm<sup>-1</sup>) at 400 nm, and k is an empirically derived constant with a value of 855 ppmw Pt/cm<sup>-1</sup> for LHG-8, LG-750, and LG-770 laser glasses [21]. Therefore values for the optical absorption of the product glass at 400 nm provide a measure of the degree of platinum dissolution during continuous melting.

The first published Pt solubility study was by Ryder and Rindone [51] on lead-alkali silicates, phosphates, and borates who report that the solubility follows the trend: phosphates ≫ borates > silicates. The work by Ryder and Rindone [51] combined with the more recent work by Izumitani et al. [34] show the effects of glass composition on platinum solubility follow the trend: phosphate > silica-phosphate ≫ fluoro phosphate ≈ borates > silicate [34,51]. Izumitani et al. [34] results are based on solubility measurements using LHG-5 and LHG-8 (phosphates), HAP-3 (silicophosphate), LHG-10 (fluorophosphate) and LSG-91H (silicate). In another study, Hayden et al. [52] examined the effects of the Al<sub>2</sub>O<sub>3</sub> concentration in phosphate glasses on Pt solubility. They chose three commercial phosphate laser glasses (LG-770, LG-760 and APG-1) each having different Al<sub>2</sub>O<sub>3</sub> content. The effects of alumina were studied because it is a common modifier added to improve thermal-mechanical properties and chemical durability [11]. These researchers [52] report that the Pt solubility decreases as the Al<sub>2</sub>O<sub>3</sub> content increases. The effects of Al<sub>2</sub>O<sub>3</sub> on Pt solubility tend to parallel those reported by Izumitani et al for SiO<sub>2</sub> in phosphate glasses [34]. The compositions of LHG-8 and LG-770 (Table 1) have been selected in part because of their Pt solubility properties under oxidizing conditions.

A model for Pt-inclusion dissolution has been reported [53]. When the temperature is sufficiently high, mass transport (molecular diffusion), rather

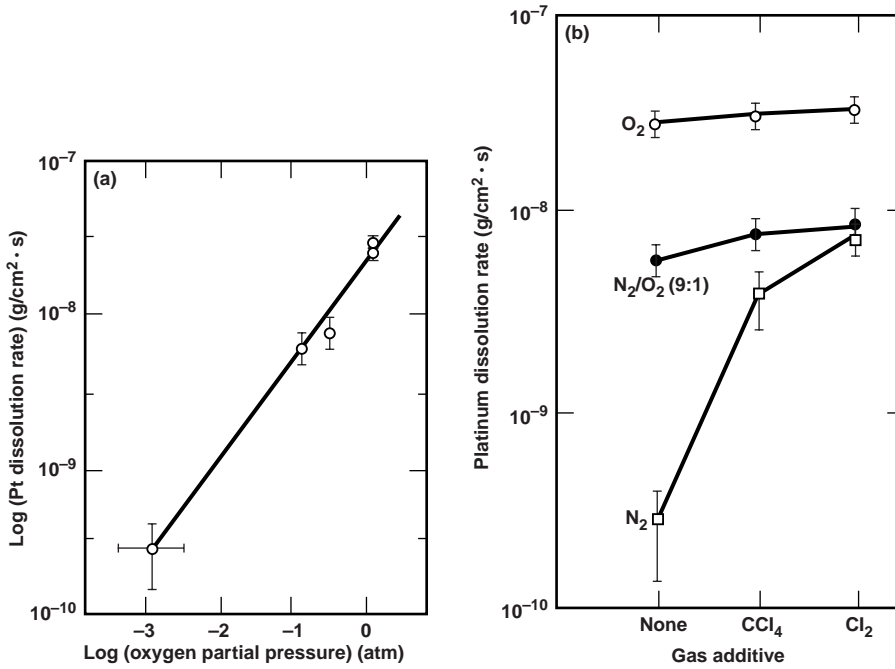


Fig. 8. Platinum dissolution rate in the metaphosphate laser glass, LHG-8 at 1200°C as a function of (a) O<sub>2</sub> partial pressure, and (b) type of chlorinated gas additive in various O<sub>2</sub> + N<sub>2</sub> gas mixtures.

than reaction kinetics, dominates the dissolution process. The time to dissolve a Pt-inclusion can be approximated by the simple expression

$$t_d = \rho_i r_0^2 / [2D(C_s - C_0)M], \quad (9)$$

where  $t_d$  is the dissolution time (s),  $\rho_i$  the inclusion material density (19 g/cm<sup>3</sup> for Pt),  $r_0$  the initial inclusion radius (cm),  $M$  the gram-atomic weight of Pt, and  $D$  is the Pt-ion diffusion constant (cm<sup>2</sup>/s).  $C_s$  and  $C_0$  refer to the Pt-ion concentration (g/cm<sup>3</sup>) at saturation and measured in the melt, respectively;  $C_s$  is about 1100 ppmw Pt<sup>n+</sup> at 1100°C in LHG-8 [53] and  $C_0$  is determined from Eq. (8). The diffusion constant for Pt<sup>n+</sup> in LHG-8 laser glass has been estimated to be about 10<sup>-7</sup> cm<sup>2</sup>/s at 1100°C [53].

The dissolution of platinum-inclusions is more difficult in continuous than discontinuous melting because of the variable melt residence time. In the discontinuous process the entire glass melt sees the same process time whereas in a continuous melter the glass experiences a distribution of residence

times. The residence time distributions depend entirely on the properties of the fluid and the geometry and degree of mixing within the melter. Therefore, to insure complete Pt-inclusion dissolution in a continuous melter requires vigorous addition of oxidizing gas.

In most cases a small number of inclusions can be tolerated if the size of the inclusion is small (<5 μm) and the laser-induced damage (i.e., fractures) they produce does not exceed 300 μm. Inspection methods have been developed and put into production to scan each piece of laser glass with the output from a pulsed laser and measure the size of any damage site generated at fluences between 7 and 14 J/cm<sup>2</sup> (laser pulse length ~8 ns) [54]. These fluences are similar to those the glass sees in operation on the megajoule laser [8].

## 6. OH removal from phosphate laser glasses

As discussed in Section 4.3, phosphate glasses react with water vapor forming chain terminating

hydroxyl groups at equilibrium concentrations that vary as  $\sqrt{P_{\text{H}_2\text{O}}}$  (see Fig. 6). These hydroxyl groups increase the rate of non-radiative decay of  $\text{Nd}^{3+}$  from the upper  ${}^4\text{F}_{3/2}$  laser level [11] and thus adversely affect laser performance.

The gases added to promote Pt-inclusion dissolution can also increase the removal of residual hydroxyl groups in the glass. The reduction of  $-\text{OH}$  in the glass by addition of either inert or reactive gases has been the subject of numerous studies (see, for example [35–38,55–57]). In particular, the addition of chlorine or chlorine-containing compounds is a well-documented method for OH removal in silicate and phosphate glasses [36,38,40,55,56].

We have developed a computer model that describes the removal of OH groups from phosphate laser glass using either an inert (e.g.,  $\text{O}_2$ ,  $\text{N}_2$ ) or reactive (e.g.,  $\text{Cl}_2$ ) gas employing reaction equilibrium and mass transfer constraints (Fig. 9). The model is based on a time-dependent, one-dimensional bubble column formulation [58] and is designed to calculate glass dehydration for either discontinuous or continuous melting operations involving one or

more interconnected processing tanks and one or more dehydrating bubble columns.

### 6.1. Equilibrium chemistry and mass transport governing dehydration

The model treats the dehydration process by a combination of mass transport and chemical equilibrium. This process was discussed in Section 4.3. The transport step involves the diffusion of a water carrying component ( $-\text{OH}$ ) from the interior of the glass liquid to a liquid/vapor interface. This interface may occur at the exposed top surface of a melt or at a bubble surface for the case in which bubbling through the melt is employed. At the interface, the model uses Eq. (1) as the governing reaction with the  $-\text{OH}$  in the liquid in equilibrium with water in the vapor phase according to the equilibrium relation

$$K_w = C_{\text{gH}_2\text{O}} / (C_{\text{mOH}})^2, \quad (10)$$

where  $K_w$  is the equilibrium constant ( $1/(\text{mol}/\text{m}^3)$ ),  $C_{\text{gH}_2\text{O}}$  the water vapor concentration in the gas

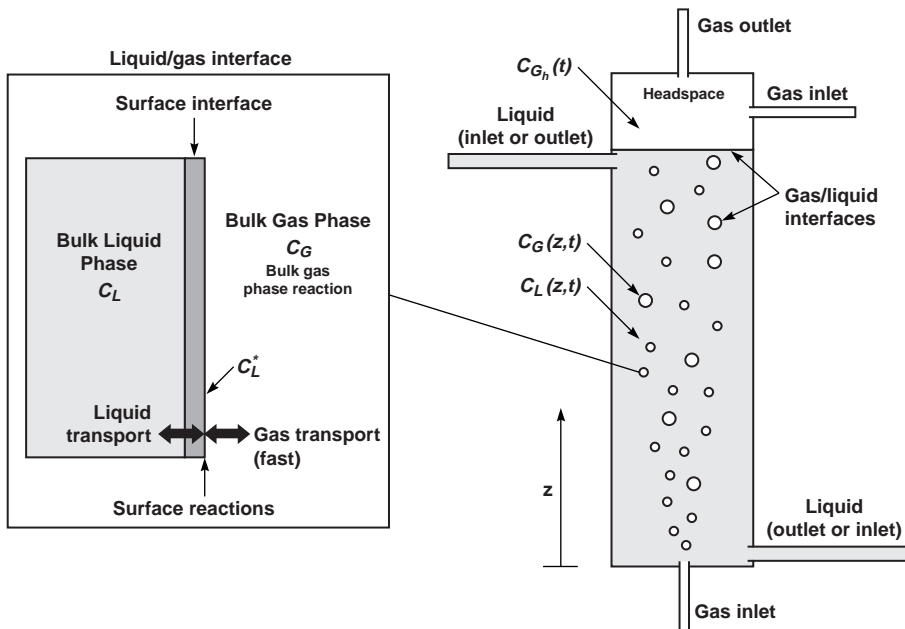


Fig. 9. Physical representation of the numerical model for OH removal using gas bubbling through a phosphate glass melt. The model treats bubbling using both inert and reactive gases.

phase (mol/m<sup>3</sup>) and C<sub>mOH</sub> the OH concentration in the melt (mol/m<sup>3</sup>).

In the presence of chlorine we add the additional vapor phase equilibrium given by Eq. (2). As written, Eq. (2) is known as the reverse Deacon reaction [42], and chlorine acts to dehydrate the vapor phase (e.g., bubble). It is assumed that the bubble contents are held near equilibrium for the reverse Deacon reaction that has an equilibrium constant given by

$$K_d = \frac{[\text{HCl}]^4[\text{O}_2]}{[\text{H}_2\text{O}]^2[\text{Cl}_2]^2}, \quad (11)$$

where the square brackets denote species concentrations (mol/m<sup>3</sup>) and K<sub>d</sub> is the equilibrium constant that has a value of 5523 and 9871 mol/m<sup>3</sup> at 1150°C and 1250°C, respectively [42]. These relatively large K<sub>d</sub> values lead to low values of water vapor in equilibrium mixtures. As a consequence, in systems containing chlorine in the bubbling gas, the concentration gradient that controls the rate of mass transfer across the liquid/gas interface remains high. In contrast, in systems where only oxygen is present the bubbles tend to reach water vapor saturation because of the equilibrium imposed by Eq. (1). In this case, the concentration gradient for transport of OH is smaller and the dehydration rate is correspondingly slower.

Mass transport across the bubble interface is computed by using an effective transport parameter, (kA), which is the product of the mass transfer coefficient, k, and the interfacial area, A. Deckwer [59] has proposed a correlation for mass transfer that can be employed over a range of bubble flow conditions; we have used this correlation in model simulations of bubble column dehydration in both discontinuous and continuous melting.

The dehydration model has been used to predict dehydration levels for both discontinuous and continuous melting processes; in Fig. 10 the computed relative OH levels are compared to measured levels in the product glass from both melting processes. The continuous melting data represent operating regimes for which the bubbling flow rate and Cl<sub>2</sub> content differed by more than 10 times and thus is a good test of the model. The ability to

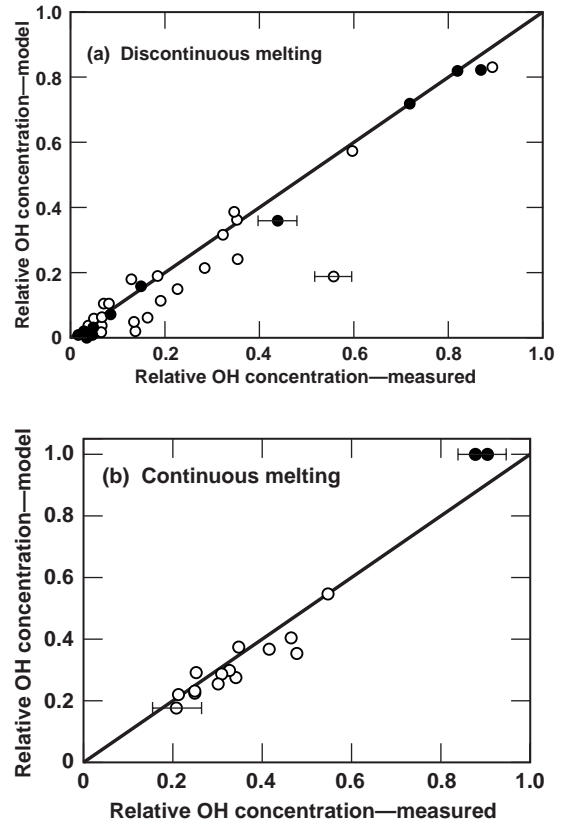


Fig. 10. Comparison of measured versus predicted OH concentrations in glass produced by (a) small-scale (<1 ℓ) discontinuous melts and (b) production-scale continuous melting operations. The solid circles are 100% oxygen bubbling only, while open circles represent bubbling with oxygen and variable amounts of chlorine (<50%).

predict the dehydration in both discontinuous and continuous melts confirms that the basic model assumptions capture the primary physics and chemistry involved in dehydration of phosphate glass by gas bubbling.

### 7. Summary and conclusion

Continuous melting has been used for the first time to prepare meter-scale plates of Nd-doped phosphate laser glass. Two laser glasses have been successfully manufactured using this process: LHG-8 and LG-770.

To meet the laser performance criteria, the glass must have high-optical quality ( $\Delta n \leq 2 \times 10^{-6}$ ), be free of Pt-inclusions, and have only trace amounts of hydroxyl group contamination. The latter two specifications require special processing features in the continuous melter system, in particular the addition of oxidizing and chlorine-containing gases into the glass melt.

Platinum inclusions are removed by dissolution in the melt under oxidizing conditions; the time to dissolve Pt-inclusions increases as the square of the inclusion diameter. The rate of Pt dissolution is highest with the use of a  $\text{Cl}_2$  and  $\text{O}_2$  mixture.

The measured equilibrium OH content in the glass depends on the square root of the surrounding water vapor pressure as expected from simple reaction equilibrium. The equilibrium constant has an approximate value of  $0.41 \text{ cm}^{-1}/\sqrt{\text{Pa}}$  at  $1300^\circ\text{C}$  in LG-770 and  $0.51 \text{ cm}^{-1}/\sqrt{\text{Pa}}$  at  $1100^\circ\text{C}$  for LHG-8.

A computational model is used to simulate dehydroxylation of the laser glass using either reactive gas (e.g.,  $\text{Cl}_2$ ) or inert gas (e.g.,  $\text{O}_2$ ) bubbling. The model accurately predicts OH removal during both discontinuous and continuous melting operations of both LHG-8 and LG-770.

## Acknowledgements

This work is supported in the US by the Department of Energy under contract W-7405-ENG-48 and in France by the Commissariat à l'Énergie Atomique (CEA). The authors gratefully acknowledge the efforts by R. Steele, S. Pucilinski, and K. Suzuki on the small-scale test melts. The authors also deeply appreciate the assistance of A. Clasen in the preparation of this manuscript.

## References

- [1] J.R. Murray, SPIE 3492 Supplement, 1998, p. 1.
- [2] M. Andre, M. Novaro, D. Schirmann, Chocs Revue Scientifique et Technique de la Direction de Applications Militaires 13 (1995) 73.
- [3] J.T. Hunt, D.R. Speck, Opt. Eng. 28 (1989) 461.
- [4] T.R. Boehly, D.L. Brown, R.S. Craxton, R.L. Keck, J.P. Knauer, J.H. Kelly, T.J. Kessler, S.A. Kumpan, S.J. Loucks, S.A. Letzring, F.J. Marshall, R.L. McCrory, S.F.B. Morse, W. Seka, J.M. Soures, C.P. Verdon, Opt. Commun. 133 (1997) 495.
- [5] A.C. Erlandson, M.D. Rotter, D.N. Frank, R.W. McCracken, Design and Performance of the Beamlet Amplifiers, ICF Quarterly Report, Lawrence Livermore National Laboratory Report UCRL-LR-105821-95-1, 1994, p. 18.
- [6] A. Erlandson, J. Horvath, K. Jancaitis, J. Lawson, K. Manes, C. Marshall, E. Moor, S. Payne, L. Pedrotti, S. Rodriguez, M. Rotter, S. Sutton, L. Zapata, S. Seznec, J. Beullier, O. Carbourdin, E. Grebot, J. Guenet, M. Guenet, X. Maille, Fusion Technol. 34 (1998) 1105.
- [7] G. Le Touzé, O. Cabourdin, J.F. Mengué, M. Guénet, E. Grebot, S. Seznec, K. Jancaitis, C.D. Marshall, L. Zapata, A. Erlandson, SPIE 3492 (1998) 630.
- [8] B.M. VanWongerghem, J.R. Murray, J.H. Campbell, D.R. Speck, C.E. Barker, I.C. Smith, D.F. Browning, W.C. Behrendt, Appl. Opt. 36 (1997) 4932.
- [9] J.H. Campbell, L.J. Atherton, J.J. DeYoreo, M.R. Kozlowski, R.T. Maney, R.C. Montesanti, L.M. Sheehan, C.E. Barker, Large-Aperture, High-Damage-Threshold Optics for Beamlet, ICF Quarterly Report, Lawrence Livermore National Laboratory Report UCRL-LR-105821-95-1, 1994, p. 52.
- [10] J.L. Emmett, W.F. Krupke, J.B. Trenholme, The Future Development of High-Power Solid State Laser Systems, Lawrence Livermore National Laboratory Report UCRL-53344, 1982, p. 1.
- [11] J. Campbell, T. Suratwala, these Proceedings, p. 318.
- [12] J.H. Campbell, SPIE CR64 (1996) 3.
- [13] J.H. Campbell, 25 Years of Laser Glass Development Leading to a 1.8 MJ, 500 TW Laser for Fusion Ignition, Lawrence Livermore National Laboratory Report, UCRL-JC-129507, 1998, p. 1.
- [14] J. Campbell, T. Suratwala, C. Thorsness, J. Hayden, A. Thorne, A. Marker, K. Takeuchi, M. Smolley, G. Ficini-Dorn, presented at 15th University Conference on Glass Science, Rolla, MO, June 1999.
- [15] Laser Glass Product Catalog, Hoya Corporation USA, Fremont, CA, 1994, p. 1.
- [16] S.E. Stokowski, R.A. Saroyan, M.J. Weber, Laser Glass Nd-Doped Glass Spectroscopic and Physical Properties, Lawrence Livermore National Laboratory Report M-095, Rev. 2, vols. 1, 2, 1981.
- [17] J. Atherton, Optics Technology for the National Ignition Facility, Lawrence Livermore National Laboratory Report UCRL-LR-105821-99-2, 1999, p. 111.
- [18] Laser Glass Product Catalog, Schott Glass Technologies, Duryea, PA, 1999, p. 1.
- [19] A.J. Marker, SPIE 531 (1985) 2.
- [20] T.S. Izumitani, Optical Glass, Am. Inst. Phys. Transl. Ser., New York, 1986, ch. 3.
- [21] J.H. Campbell, E.P. Wallerstein, J.S. Hayden, D.L. Sapak, D.E. Warrington, A.J. Marker, H. Toratani, H. Meissner, S. Nakajima, T. Izumitani, Elimination of Platinum Inclusions in Phosphate Laser Glasses, Lawrence Livermore National Laboratory Report UCRL-53932, 1989, p. 1.

- [22] H. Bach, N. Neuroth, *The Properties of Optical Glass*, Springer, Berlin, 1995.
- [23] H. Toratani, PhD thesis, Kyoto University, Kyoto, 1989, p. 1.
- [24] S.E. Stokowski, D. Krashkevich, *Mater. Res. Soc. Symp.* 61 (1986) 273.
- [25] D. Sapak, J. Ward, J. Marion, *SPIE* 970 (1988) 107.
- [26] P. Ehrmann, J.H. Campbell, T.I. Suratwala, J.S. Hayden, D. Krashkevich, K. Takeuchi, these Proceedings, p. 251.
- [27] F.A. Cotton, G. Wilkinson, *Advanced Inorganic Chemistry*, 5th Ed., Wiley, New York, 1988, p. 962.
- [28] A.R. Cooper, in: T.D. McGee (Ed.), *Proceedings of the Educational Symposium on Refractories in Slagging Environments*, Amer. Ceram. Soc., 1981, p. 1063.
- [29] *Fundamentals of Damage in Laser Glass*, National Materials Advisory Board, Division of Engineering, National Research Council NMAB-271, 1970, p. 1.
- [30] R.W. Hopper, D.R. Uhlmann, *J. Appl. Phys.* 41 (1970) 4023.
- [31] R. Gonzales, D. Milam, *Laser Induced Damage in Optical Materials: National Bureau of Standards (special publication)*, 745, 1988, p. 128.
- [32] J.H. Campbell, E.P. Wallerstein, J.S. Hayden, D.L. Sapak, D.E. Warrington, A.J. Marker, *Glastech. Ber. Glass Sci. Technol.* 68 (1995) 11.
- [33] J.H. Campbell, E.P. Wallerstein, H. Toratani, H.E. Meissner, S. Nakajima, T.S. Izumitani, *Glastech. Ber. Glass Sci. Technol.* 28 (1995) 59.
- [34] T. Izumitani, M. Matsukawa, H. Miyade, *Laser Induced Damage in Optical Materials, National Institute of Standards and Technology (special publication)*, 756, 1988, p. 29.
- [35] R. Adams, *Phys. Chem. Glasses* 2 (1961) 50.
- [36] J. Chun, Z. Junzhou, Z. Dunshui, *Chin. J. Lasers A* 23 (1996) 182.
- [37] F. Gomez, P. Vast, P. Llewellyn, F. Rouquerol, *J. Non-Cryst. Solids* 222 (1997) 415.
- [38] T. Elmer, *Glastech. Ber. Glass Sci. Technol.* 61 (1988) 24.
- [39] E. Boulos, N. Kreidl, *J. Canadian Ceram. Soc.* 41 (1972) 83.
- [40] J. Shelby, *Handbook of Gas Diffusion in Solids and Melts*, ASM International, Materials Park, OH, 1996, p. 217.
- [41] H. Ebendorff-Heidepriem, D. Ehrt, *Glastech. Ber. Glass Sci. Technol.* 68 (1995) 139.
- [42] C.W. Arnold, K.A. Kobe, *Chem. Eng. Prog.* 48 (1952) 266.
- [43] R.B. Bird, W.E. Stewart, E.N. Lightfoot, *Transport Phenomena*, Wiley, New York, 1960.
- [44] *Schott Optical Glass Catalog*, Schott Glass Technologies, Duryea, PA, 1992.
- [45] *Hoya Optical Glass Technical Data*, Hoya Corporation USA, Fremont, CA, 1990.
- [46] D. Malacara, S.L. DeVore, in: D. Malacara (Ed.), *Optical Shop Testing*, Wiley, 1992, p. 455.
- [47] J.H. Campbell, G. Edwards, F. Frick, D.S. Gemmell, K.S. Jancaitis, E.S. Jessop, M.K. Fong, R.E. Lyons, J.E. Murray, H.G. Patton, J.H. Pitts, H.T. Powell, M.O. Riley, E.P. Wallerstein, C.R. Wolfe, B.W. Woods, *Laser Induced Damage in Optical Materials: National Institute of Standards and Technology (special publication)*, 752, 1988, p. 19.
- [48] D.C. Brown, *High-Peak-Power Nd: Glass Laser Systems*, Springer, New York, 1981, p. 276.
- [49] E.P. Plueddemann, *Silane Coupling Agents*, Plenum, New York, 1991.
- [50] G.E. Rindone, J.L. Rhoads, *J. Am. Ceram. Soc.* 39 (1956) 173.
- [51] R.J. Ryder, J.L. Rindone, *J. Am. Ceram. Soc.* 41 (1958) 415.
- [52] Y.T. Hayden, J.H. Campbell, S.A. Payne, G.D. Wilke, *Ceramic Translations: Solid-State Optical Materials*, in: A.J. Bruce, B.V. Hiremath (Eds.), *Amer. Ceram. Soc., Westerville OH*, 28, 1992, p. 283.
- [53] J.H. Campbell, *Glastech. Ber. Glass Sci. Technol.* 68 (1995) 96.
- [54] J.H. Campbell, S. Schwartz, J.F. Kimmons, *Analysis of Composition and Structure of Glass and Glass Ceramics*, Schott Series on Glass and Glass Ceramics, vol. 7, Springer, 1999 (Chapter 5.5) in press.
- [55] T. Elmer, *J. Am. Ceram. Soc.* 64 (1980) 150.
- [56] Z. Dunshui, X. Wenjuan, J. Yasi, *Chin. J. Lasers* 12 (1985) 173.
- [57] C.J. Brinker, G.W. Scherer, *The Physics and Chemistry of Sol-Gel Processing*, Academic Press, San Diego, 1990.
- [58] C.Y. Wen, L.T. Fan, *Model for Flow Systems and Chemical Reactors*, Marcel Dekker, New York, 1975, p. 175.
- [59] W.D. Deckwer, A. Schumpe, *Chem. Eng. Sci.* 48 (5) (1993) 889.